Short Communication

For reprint orders, please contact: reprints@futuremedicine.com

Nanomedicine

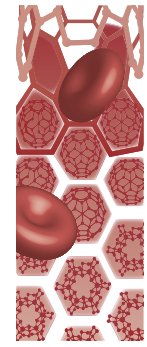

Anticancer of palladium-doped magnesia nanoparticles: synthesis, characterization, and *in vitro* study

Mohamed Qasim Al-Fahdawi[1], Abdullah Rasedee*[,1,2], Faris AJ Al-Doghachi[3], Rozita Rosli[1], Yun Hun Taufiq-Yap[4,5] & Mothanna Sadiq Al-Qubaisi[1]

[1]Institute of Bioscience, Universiti Putra Malaysia, Serdang, Selangor 43400 UPM, Malaysia

[2]Department of Veterinary Pathology & Microbiology, Faculty of Veterinary Medicine, Universiti Putra Malaysia, Serdang, Selangor 43400 UPM, Malaysia

[3]Department of Chemistry, Faculty of Science, University of Basra, Basra, Iraq

[4]Catalysis Science & Technology Research Centre, Faculty of Science, Universiti Putra Malaysia, Serdang, Selangor 43400 UPM, Malaysia

[5]Department of Chemistry, Faculty of Science; Universiti Putra Malaysia, Serdang, Selangor 43400 UPM, Malaysia

*Author for correspondence: Tel.: +603 8946 3455; Fax: +603 8946 1971; rasedee@upm.edu.my

Aim: To prepare, physicochemically characterize and determine the anticancer of palladium-doped magnesia (Pd/MgO) nanoparticles. **Materials & methods:** Pd/MgO nanoparticles were prepared by the co-precipitation method from the aqueous solution of $Mg(NO_3)_2.6H_2O$ using K_2CO_3 and the impregnation of MgO into palladium acetylacetonate. **Results:** Pd/MgO nanoparticles were between 47 and 70 nm in size, cuboid in shape and tended to form aggregates. Nanoparticles were more antiproliferative toward cancer than the normal cells. In cancer cells, Pd/MgO nanoparticles induced apoptosis by increasing caspase activities and stimulating cytochrome C release. The anticancer effects of Pd/MgO nanoparticles were accentuated by the upregulation of Bax and p53 and downregulation of Bcl-2 protein expressions. **Conclusion:** Pd/MgO nanoparticles have potential to be developed as an anticancer compound.

First draft submitted: 1 May 2019; Accepted for publication: 25 July 2019; Published online: TBC

Keywords: apoptosis • cytotoxicity • mitochondrial pathway • noble metals • palladium-doped magnesia nanoparticles

Cancer, or malignant tumor, is a disease caused by abnormal cell growth. Excessive proliferation of cancer tissue cells eventually damages neighboring healthy cells and tissues with lethal outcomes. Cancer is in fact, one of the deadliest and most complicated diseases in medicine; the result of mutations in DNA responsible for the synthesis of cellular proteins. The DNA abnormalities cause production of abnormal proteins that are harmful to the organism [1,2]

Cancer treatments have evolved from surgical removal, chemotherapies, radiotherapy and immunotherapy to the use of innovative nanoparticulated drug delivery systems with sustained effect and controlled release characteristics. These delivery systems have several advantages over pure chemotherapeutics by protecting the loaded compounds or drugs from degradation while improving their solubility, stability, and targeted delivery [3,4].

The use of noble metals in the treatment of cancers began approximately four decades ago [5,6]. Noble metals shown to have anticancer effects include platinum, ruthenium, rhodium, iridium, gold , and silver [7]. Among noble metal therapeutic compounds already marketed for treatment of cancers are the platinum-based derivatives, cisplatin, carboplatin and oxaliplatin. Cisplatin, for example was shown to target DNA [8], RNA [9], mitochondria [10] and functional proteins [11,12]. Cisplatin can also passively or actively penetrate tumor cells, and interacts with DNA to inhibit cell proliferation [13].

The microenvironment of cancer tissues is relatively more acidic than that of normal tissues [14]. Since palladium-doped magnesia (Pd/MgO) dissociates at low pH [15], resulting in the release of palladium from the complex, the acidic cancer tissue microenvironment would facilitate delivery of the metal to exert its therapeutic effect. Pd/MgO nanoparticles can also offer an improved and targeted tumor therapeutic strategy while showing less toxic effects on normal tissues than conventional chemotherapeutics. However, at this juncture, the full potential of the Pd/MgO

Future Medicine

nanoparticles as an anticancer agent is yet to be determined. In this study, Pd/MgO nanoparticles were developed, characterized and their anticancer properties determined *in vitro*.

Materials & methods

Chemicals & reagents

Trypsin/ethylenediamine tetracetic acid (EDTA) solution was purchased from Invitrogen (CA, USA). Dimethyl sulfoxide (DMSO), phosphate-buffered saline (PBS), 3-(4,5-dimethylthiazol-2-yl)-2,5-diphenyltetrazolium bromide (MTT), Dulbecco's modified Eagle's medium (DMEM), diphenylamine (DPA) reagent (100 ml glacial acetic acid 1.5 g diphenylamine, 1.5 ml concentrated sulfuric acid 0.5 ml and 16 mg/ml acetaldehyde stock) and trypan blue dye were purchased from Sigma Chemical Company (Perth, WA, Australia).

Preparation of Pd/MgO nanoparticles

The Pd/MgO nanoparticles were prepared using the precipitation method as described previously [16]. MgO was prepared using a 0.1 M aqueous solution of $Mg(NO_3)_2.6H_2O$ (Merck; >99.0%) and 1 M K_2CO_3 (Merck, Darmstadt, Germany; >99.7%) as precipitants. The sample (precipitant) was filtered and washed with hot water and dried at 120°C for 12 h. Subsequently, the dried samples were precalcined in air at 500°C for 5 h to remove CO_2. The sample was then pressed into discs at 600 kg/m^2 (Hydrolic for KBr disc) and calcined at 1150°C for 20 h for the enhancement of mechanical properties.

The sample was impregnated with 5% Pd using $Pd(C_5H_7O_2)_2$. H_2O, (Acros Chemicals; >99%), dissolved with dichloromethane for 5 h to produce $Pd(acac)_2$/MgO. After impregnation in air, the samples were dried for 12 h at 120°C, crushed and sieved (250 µm) to obtain particles of 80–150 or 150–250 µm in diameter. Finally, the Pd^{2+} phase nanoparticles were reduced to metal Pd° phase at the active site of the nanoparticles using 5% H_2/Ar to produce Pd/MgO nanoparticles.

Physicochemical properties of nanoparticles

Scanning electron microscopy & energy dispersive x-ray spectroscopy

Scanning electron microscopy (SEM, Model LEO 1450VP [LEO Electron Microscopy Ltd. Cambridge, UK]), with an accelerating voltage of 30 kV, and energy dispersive x-ray spectroscopy (EDX) were used to determine the morphology and elemental composition of powdered nanoparticles, respectively. The samples were degassed in an evacuated heated chamber at 100°C overnight. Prior to SEM scanning, dried samples were spread over double-sided conductive tape adhered to the specimen stub.

Transmission electron microscopy

Transmission electron microscopy (TEM, Hitachi H-7100, Japan) was used to determine the fine structure of the crystals. The nanoparticle powder was disseminated in deionized water, placed onto carbon-cover copper grids on filter paper and dried at room temperature before viewing.

X-ray diffraction

The x-ray diffraction (XRD) characterization of nanoparticle powder was performed using the Shimadzu diffractometer model XRD 6000, Japan. The analysis employed the Cu-K_α radiation generated by a Philips glass diffraction x-ray tube broad focus 2.7 kW type at ambient temperature. The crystallite size D of the samples was calculated by the Debye–Scherrer's relationship according to standard procedures [17,18] using the following formula:

$$T = 0.9\,\lambda / (\beta \cos\theta)$$

where T is the crystallite size, λ is the incident x-ray wavelength, β is the full width at half-maximum, and θ is the diffraction angle.

Fourier transform infrared

Fourier transform infrared (FTIR) spectra for powdered nanoparticles were recorded over the range of 400–4000 cm^{-1} on a Smart Orbit spectrometer (Thermo Nicolet Nexus, USA) using a sample of approximately 1% in 200 mg of spectroscopic-grade potassium bromide (KBr) with 10 tons of pressure.

Thermogravimetric analysis

The thermal strength of the nanoparticles was investigated using the Mettler Toledo TG-SDTA apparatus (Pt crucibles, Pt/Pt– Rh thermocouple) (Switzerland), with a purge gas (nitrogen) flow rate of 30 ml min^{-1} and a heating rate of 10°C min^{-1} from room temperature to 1000°C.

Brunauer, Emmett & Teller analysis

The total surface area of the nanoparticles was evaluated via nitrogen adsorption at -196°C. The evaluation was performed using a nitrogen adsorption-desorption analyser (Surfer Analyser, Milan, Italy).

Cell culture

Four human cell lines, colorectal adenocarcinoma (HT29), lung carcinoma (A549), normal colon (CCD-18Co) and normal lung (MRC-5) cells, all virus-negative, were obtained from the American Type Culture Collection (ATCC; MD, USA). The cells were cultured in DMEM (Sigma Aldrich, MO, USA) supplemented with 10% FBS and 1% penicillin (100 U/ml) (Isocillin, Aventis, Germany) in an incubator at 37°C in the presence of 5% CO_2.

3-(4,5-dimethylthiazol-2-yl)-2,5-diphenyltetrazolium bromide assay

The Pd/MgO nanoparticles were mixed well in DMEM medium (Sigma Aldrich) containing fresh 10% heat-inactivated FBS and nanoparticle colloidal suspension was obtained using ultrasound method [17,18]. Two hundred microliters of 5×10^3 cells/ml suspension were added to each well of a 96-well cell culture plate to a final concentration 1×10^3 cells/well. The media was aspirated and replaced with 200 µl fresh media containing nanoparticles of concentrations ranging from 1.56 to 100 µg/ml, and chemotherapeutic agents (oxaliplatin for HT29 and CCD-18Co cells, and paclitaxel for A549 and MRC-5 cells) ranging from 0.156 to 10.0 µg/ml. The last row was used for the nontreated control. The plate was then incubated at 37°C under 5% CO_2, for 24 h. The medium was aspirated and the cells washed with PBS buffer trice to remove the test compounds, and fresh medium added. Then, 200 µl of 5 mg/ml 3-(4,5-dimethylthiazol-2-yl)-2,5-diphenyltetrazolium bromide (MTT) solution was added to each well and the plate incubated for 4–6 h at 37°C under 5% CO_2. The MTT-containing medium was then carefully removed and replaced with 200 µl DMSO/well, to dissolve the formazan crystals. The plates were read on automated spectrophotometric EL 340 multiplate reader (Bio-Tek Instruments, Inc., VT, USA) at 570 nm. The viability percentage is calculated by:

$$(OD_{\text{treated well}}) / (OD_{\text{nontreated well}}) \times 100.$$

OD refers to optical density

For each test compound and cell line, the 24 h IC_{50} values (50% cell growth inhibition concentration) were determined from the dose–response curves.

Caspases

The effect of treatment on HT29 and A549 cell caspase-3, -8 and -9 activities was determined using commercial colorimetric assay kits (Promega, WI, USA) in accordance with recommended protocol.

Quantification of Bax, p53, Bcl-2 & cytochrome C protein assay

The expressions of p53, Bax, Bcl-2 and cytochrome C proteins in HT29 and A549 cells treated with Pd/MgO nanoparticles were determined using the ELISA assay kits (R&D Systems, MN, USA).

Microscopic examination of cell morphology

Two milliliters of cell suspension were seeded into six-well plates to contain 1×10^4 HT29 or A549 cells/well and treated with Pd/MgO nanoparticles at the predetermined IC_{50} concentrations. The cells were examined under a light inverted microscope for morphological assessment.

Statistical analysis

All experiments were done in three triplicates. Data were expressed as means ± S.D. All statistical analyses were performed using Minitab statistical software (Minitab, Inc., PA, USA). Treatment effects were determined using

one-way analysis of variance (ANOVA) followed by Tukey's *post hoc* analysis. A value of $p < 0.05$ was considered significant unless otherwise indicated.

Results

Material characterization

Morphological & elemental analysis of nanoparticles

Scanning electron microscopy & EDX

The SEM and EDX micrographs for the pure Pd/MgO samples are shown in Figures 1A and 2, respectively. The strong interaction among nanoparticles caused the Pd/MgO nanoparticles to form aggregates.

Transmission electron microscopy

The TEM images of Pd/MgO nanoparticles are shown in Figure 2B. It seemed that the Pd/MgO nanoparticles like the Pt/MgO are cuboid but with nanosize range of 60–79 nm and averaging at 70 nm. Most of the Pd/MgO nanoparticles were in aggregates, which is attributed to the electrostatic interaction between nanoparticles. This behavior indicates that there were strong interactions among nanoparticles, which is consistent with the SEM findings.

Crystallinity

The patterns generated by XRD instrument for Pd/MgO nanoparticles are shown in Figure 2C. High temperature calcination is essential for the development of the catalytically active cuboid phase of magnesium oxide. Magnesium oxide crystallized at 500°C. According to data obtained from powder XRD for the Pd/MgO nanoparticles calcined at 600°C, the magnesium oxide comprises of a cuboid system. The sharp peaks located at about $2\theta = 37.0°$ (111), 43.1° (200), 62.3° (220), 74.8° (311) and 78.9° (222) are attributed to the cuboid crystalline form of magnesium oxide (JSPDS file no.: 01-081-1545). The x-ray diffraction pattern for palladium that has been incorporated onto the surface of magnesium oxide showed stable cuboid Pd, located at $2\theta = 2\theta = 40.0°$ (111), 46.5° (200) and 68.5° (220) (JSPDS file no.: 01-081-1545). The size of the Pd/MgO crystals determined with the Debye–Scherrer's equation was 47.3 nm. The BET specific surface area (S_{BET}), pore volume and pore radius of the Pd/MgO nanoparticles were 15.7 m^2/g, 0.2122 Cm^3/g and 11.4°A, respectively. The calculated pore volume-to-S_{BET} ratio was 13.5 10^{-9} m.

Infrared absorption bands

In Figure 2D, the peaks at 2936 and 1733 cm^{-1} in the FTIR spectrum represent a weak C–H and a strong C=O stretching, respectively, which are attributed to chemical residues from nanoparticle preparation. On the other hand, the peak at 3562 cm^{-1} represents vibrational bands, which is due to moisture in the Pg/MgO nanoparticle sample. The peaks at approximately 3154 and 1583 cm^{-1} represent the stretching and bending modes, respectively, of hydroxyl groups. Although the sample was subjected to high temperature calcination, the appearance of these modes signifies that the Bronsted acid-active sites were present on the surface of Pd/MgO nanoparticles. The band at 3780 and 1442 cm^{-1} corresponds to the stretching vibration and bending, respectively, of -OH bonded to Mg. The bands at 1369, 1238, and 1165 cm^{-1} correspond to bending of C-H bonds in CH_3, stretching of C–C, and bending of C–H, respectively. The band at 1005 and 855 cm^{-1} corresponds to C–O bond.

Thermogravimetric analysis

Figure 2E shows the thermogravimetric curve for Pd/MgO nanoparticles. From the curve, the weight loss was estimated at 2%, occurring in the temperature range of 100–300°C. This weight loss may be attributed to loss of moisture from the Pd/MgO nanoparticle sample. The study shows that calcination of Pd/MgO nanoparticles at a temperature range of 25–400°C caused elimination of not only physically adsorbed water, but also loss of nitrogen oxide gases, and the transformation of $MgO(OH)_2$ to palladium. The second mass loss began at approximately 680 and ended at 1000°C. This loss of mass is attributed to the degradation of carbon residue to CO_2 gas.

Anticancer of Pd/MgO nanoparticles

Cytotoxicity

The toxic effect of Pd/MgO nanoparticles on the CCD-18Co, MRC-5, HT29 and A549, was determined by MTT assay. The toxic effect of Pd/MgO nanoparticles on the HT29 and A549 cells increased exponentially with increase

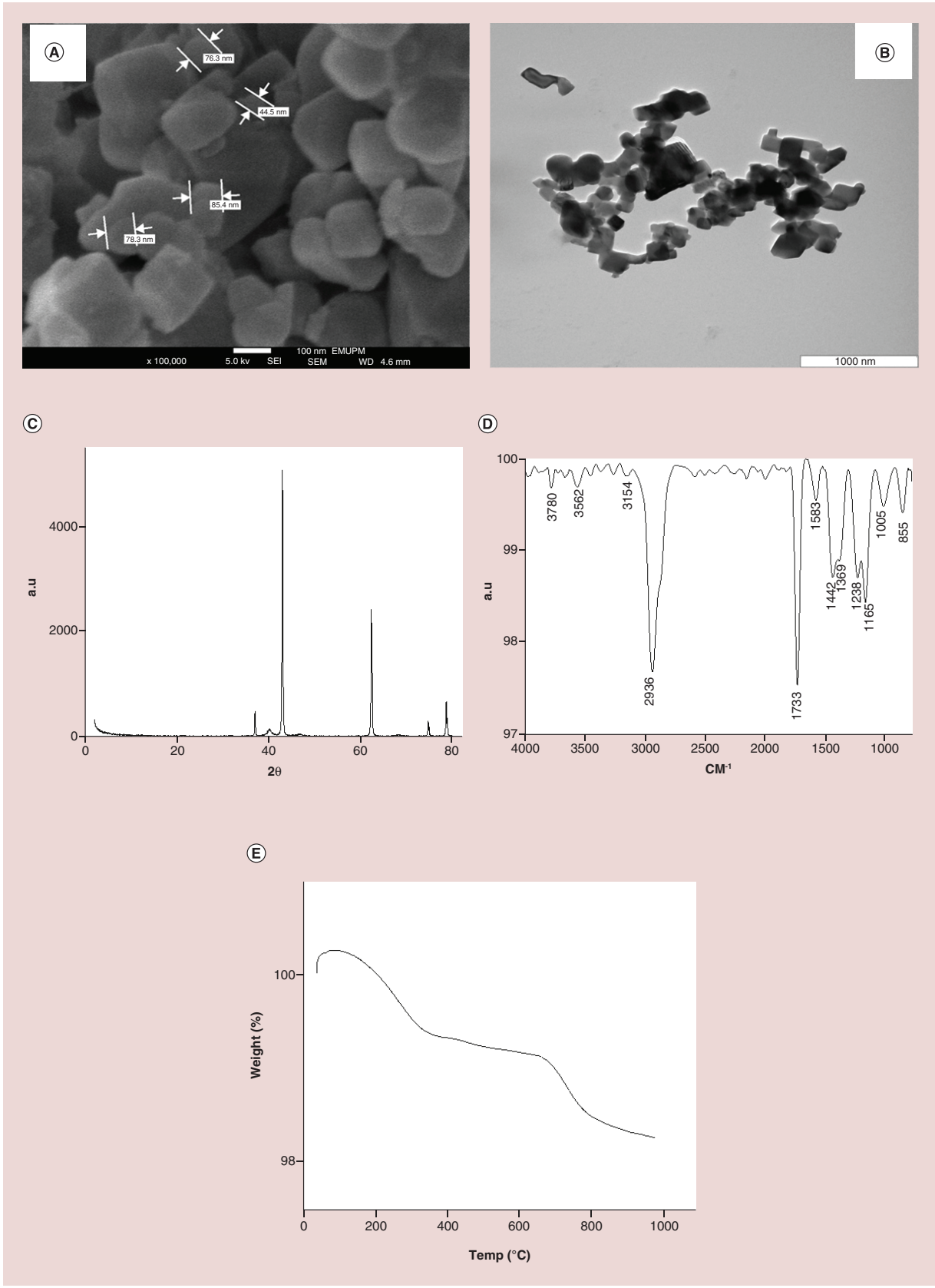

Figure 1. Characterization of Pd/MgO nanoparticles by: (A) Scanning ultramicroscopic structure of pure palladium-doped magnesia (Pd/MgO) nanoparticles. The nanoparticles were well dispersed and sizes ranged from 41 to 65 nm. **(B)** Transmission ultramicroscopic structure of pure Pd/MgO nanoparticles. **(C)** X-ray diffraction pattern of Pd/MgO nanoparticles. The data shows that Pd/MgO nanoparticles were well-formed with definitive structural and phase purity. **(D)** Fourier transform infrared spectrum of Pd/MgO nanoparticles. **(E)** Thermograph of the Pd/MgO nanoparticles showing phase with thermal treatments.

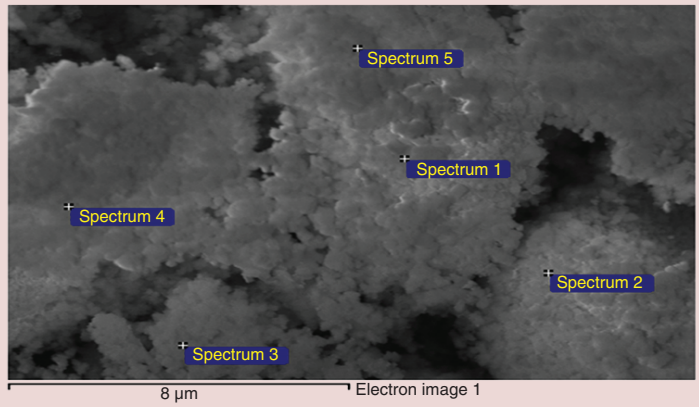

Pd-NP	In stats.	CO	O	Mg	Pd	Total
Spectrum 1	Yes	6.10	49.85	31.21	12.84	100.00
Spectrum 2	Yes	9.43	39.16	48.58	2.83	100.00
Spectrum 3	Yes	9.33	47.82	39.99	2.87	100.00
Spectrum 4	Yes	8.42	51.28	32.97	7.33	100.00
Spectrum 5	Yes	6.96	54.23	33.72	5.08	100.00
Mean		8.06	48.47	37.29	6.19	100.00

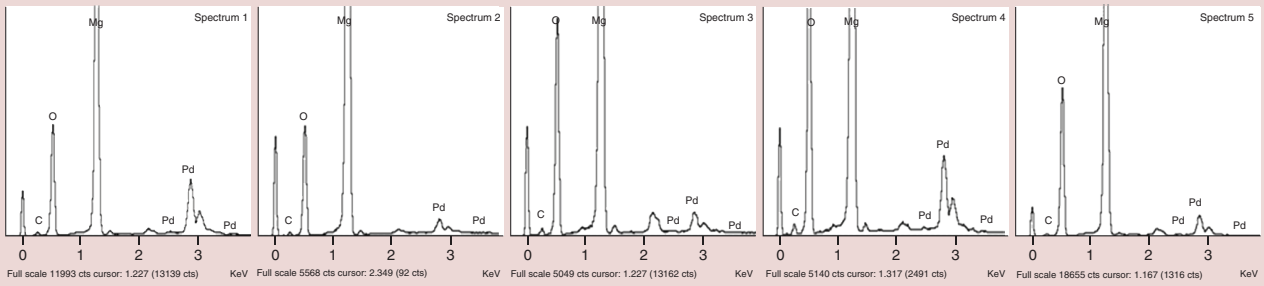

Figure 2. Energy dispersive x-ray spectroscopy of pure Palladium-doped magnesia nanoparticles. Cross-sectional scanning electron microscopy-energy dispersive x-ray spectroscopy mapping demonstrating that the composition of the fine-grain layer resulting from the powdering of palladium-doped magnesia nanoparticles is comprised mostly of palladium-doped magnesia with no signal from pure Pd alone or, MgO alone. Thus, the original raw materials are absent in the final produced nanoparticle.
NP: Nanoparticle.

Table 1. IC_{50} values of Palladium-doped magnesia nanoparticles, oxalipatin and paclitaxel on human normal colon (CCD-18Co) and cancer (HT29) cells and human normal lung (MRC-5) and cancer (A549) cells at 24 h of treatment.

Treatment	IC_{50} (µg/ml)			
	CCD-18Co	MRC-5	HT29	A549
Pd/MgO	51.6 ± 4.9	24.8 ± 3.1	22.9 ± 3.6	21.8 ± 3.8
Oxaliplatin	10.5 ± 8.1	-	4.7 ± 0.0	-
Paclitaxel	-	0.8 ± 1.6	-	0.12 ± 0.1

A549: Human breast adenocarcinoma; CCD-18Co: Human normal colon cell line; HT29: Human colorectal adenocarcinoma cell line; MRC-5: Human normal pulmonary embryonic fibroblast; Pd/MgO: Palladium-doped magnesia.

in treatment concentration (Figure 3). Normal human colon, CCD-18Co, cells showed a nonsignificant ($p > 0.05$) decrease in viability at low Pd/MgO nanoparticle concentrations. The IC_{50} value of Pd/MgO nanoparticles on CCD-18Co cells was two-times greater than on HT29 cells (Table 1). The estimated 24-h IC_{50} for Pd/MgO

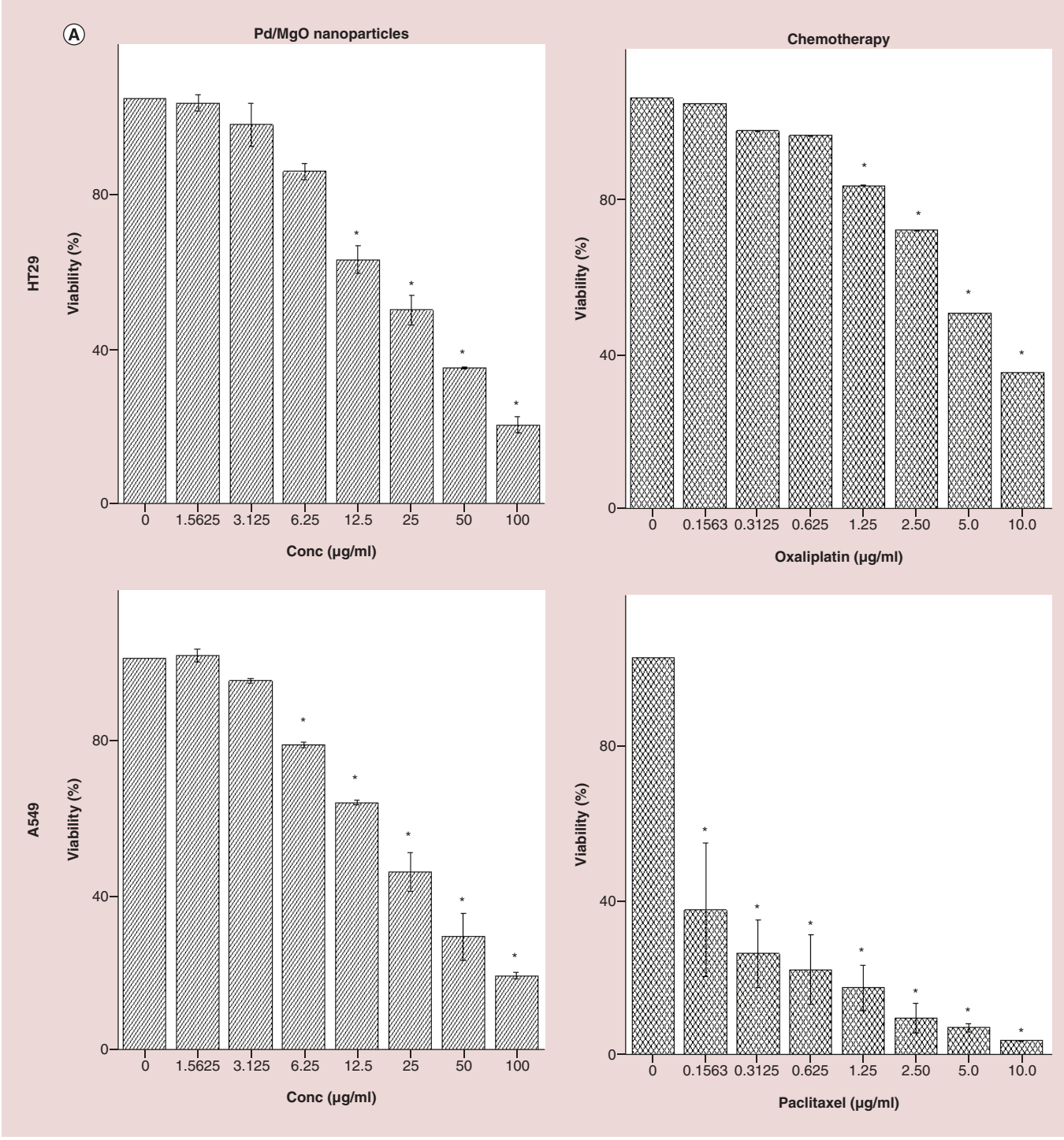

Figure 3. Effect of Pd/MgO nanoparticles and chemotherapeutics on the cell viability determined by the 4,5-dimethylthiazol-2-yl)-2,5-diphenyltetrazolium bromide assay. Mean ± standard deviation (n = 3 wells/treatment).
*$p < 0.05$ compared with the nontreated cells.
A549: Human breast adenocarcinoma; CCD-18Co: Human normal colon cell line; HT29: Human colorectal adenocarcinoma cell line; MRC-5: Human normal pulmonary embryonic fibroblast.

10.2217/nnm-2019-0178

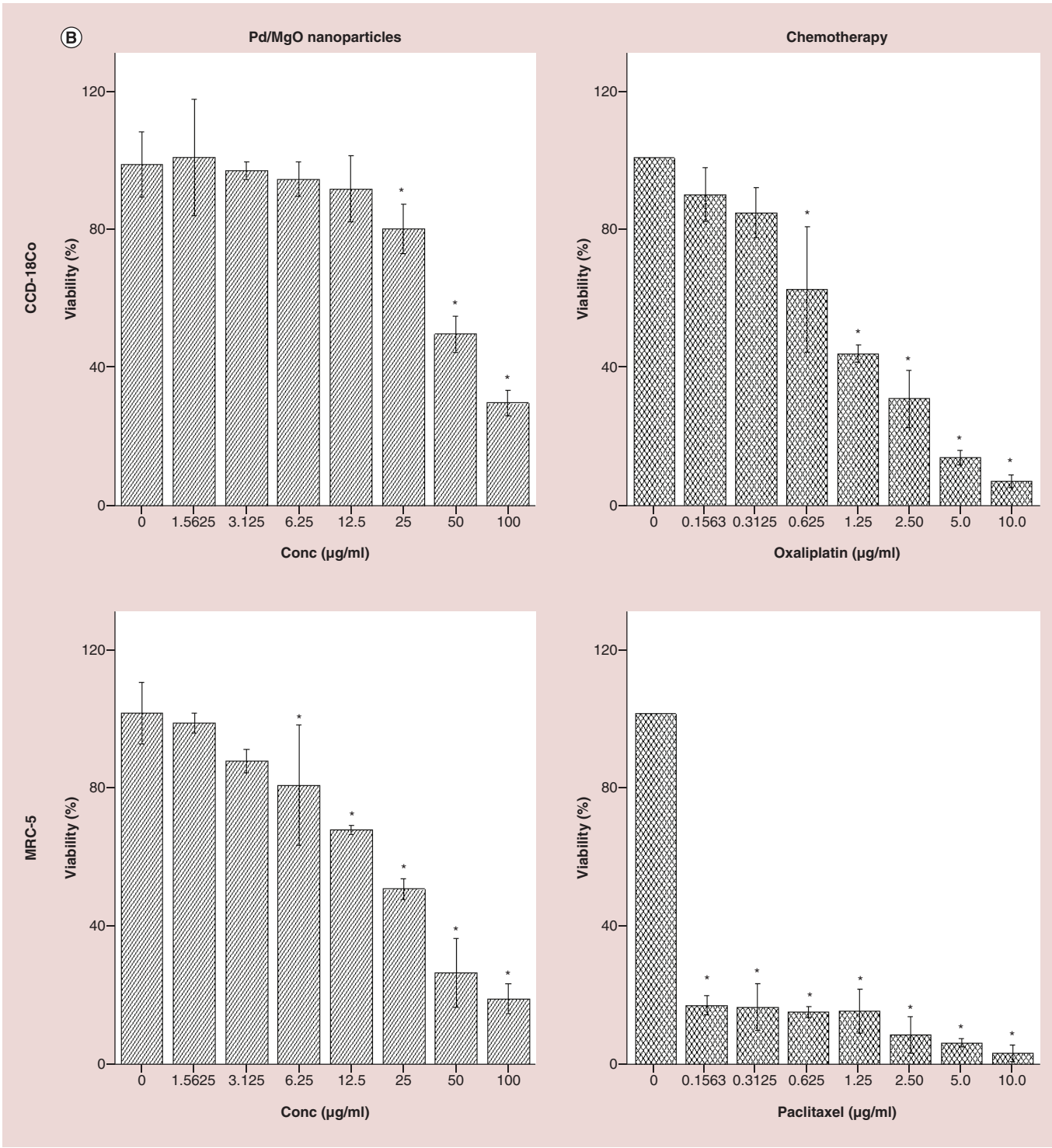

Figure 3. Effect of (cont.). Pd/MgO nanoparticles and chemotherapeutics on the cell viability determined by the 4,5-dimethylthiazol-2-yl)-2,5-diphenyltetrazolium bromide assay. Mean ± standard deviation (n = 3 wells/treatment).
*$p < 0.05$ compared with the nontreated cells.
A549: Human breast adenocarcinoma; CCD-18Co: Human normal colon cell line; HT29: Human colorectal adenocarcinoma cell line; MRC-5: Human normal pulmonary embryonic fibroblast.

nanoparticles on the cancer cells ranged between 21 and 23 μg/ml. The Pd/MgO nanoparticles were toxic to the normal lung, MRC-5, cells. Treatment with 12.5 μg/ml Pd/MgO nanoparticles caused approximately 8 and 34% lower rate of CCD-18Co and MRC-5 cell growth than the nontreated control cells, respectively, after 24-h incubation. However, under the same conditions, incubation of these cells with 25 μg/ml Pd/MgO nanoparticles, resulted in 19 and 50% lower rate cell growth, respectively, at the same time points. The A549 cells were the most sensitive to antiproliferative effect of paclitaxel. Overall, the effects of Pd/MgO nanoparticles and oxaliplatin on HT29 cells were similar, decreasing cell viability with increasing treatment concentrations (Figure 3).

Caspase-3, -8 & -9

Caspase-3

The HT29 and A549 cells after treatment with Pd/MgO nanoparticles, at all concentrations, for 12 and 24 h, showed significantly ($p < 0.05$) greater caspase-3 activities than the nontreated cells (Figure 4). The activity of this enzyme increased with increase in treatment concentrations. However, after 12 h of treatment, the anticancer effects of Pd/MgO nanoparticles were more prominent on the A549 than HT29 cells. At the same treatment period, the caspase-3 activities in the HT29 (696%) and A549 (692%) cells lines treated with 12.5 μg/ml Ag/MgO nanoparticles, were markedly higher than in nontreated cells.

Caspase-8

Unlike caspase-3, the caspase-8 activity in the tumor cells did not change significantly ($p > 0.05$) with treatment (Figure 4). However, the activity of caspase-8 in the lung cancer, A549, cells was shown to be higher than in nontreated cells by 1.34-fold after 24 h. Similar effect was not observed in the HT29 cells, suggesting that Pd/MgO nanoparticles is a more effective antiproliferative agent for A549 than HT29 cells.

Caspase-9

The activity of caspase-9 in colon cancer, HT29, cell line after treatment with 12.5 μg/ml Pd/MgO nanoparticle was approximately threefold higher than in nontreated cells after 12 and 24 h (Figure 4). In the A549 cells treated with Pd/MgO nanoparticles, the activity of caspase-9 rose quickly after 12-h exposure, to approximately fivefold higher than in nontreated cells. By 24 h, the caspase-9 activity in treated A549 cell decreased again to only approximate twofold higher than nontreated cells. The study shows that Pd/MgO nanoparticles increased caspase-9 activity in A549 cells more rapidly than in HT29 cells.

Bcl-2, Bax, p53 & cytochrome C proteins

Bcl-2

Pd/MgO nanoparticles at 12.5 μg/ml were more effective at downregulating the Bcl-2 protein expression in A549 than HT29 cells. This was observed at both the 12- and 24-h exposure periods. The A549 cell Bcl-2 expression decreased to approximately 34% of the nontreated cells. In the Pd/MgO nanoparticle-treated HT29, the expression of Bcl-2 decreased to between 78 and 80% of the nontreated cells (Figure 5).

Bax

The HT29 cell Bax protein expression after treatment with 12.5 μg/ml Pd/MgO nanoparticles increased by more than 316%, which was between two- to threefold higher than that produced by 6.25 and 3.125 μg/ml Pd/MgO nanoparticles (Figure 5). The upregulation of Bcl-2 protein in Pd/MgO nanoparticle-treated A549 cells was less significant than in the HT29 cells. These effects of Pd/MgO nanoparticle on cancer cells Bax expression were gradual and concentration-dependent.

p53

P53 protein expression in HT29 and A549 cancer cells treated with 12.5 μg/ml Pd/MgO nanoparticles was four- to sevenfold higher that in nontreated cells (Figure 5). However, in the HT29 cells, at 12 h, the p53 protein expression became significant higher ($p < 0.05$) even after treatment with 3.125 μg/ml Pd/MgO nanoparticles. It appears that the effect of Pd/MgO nanoparticles is concentration-dependent and there is no observable difference in effect between HT29 and A549 cells.

10.2217/nnm-2019-0178

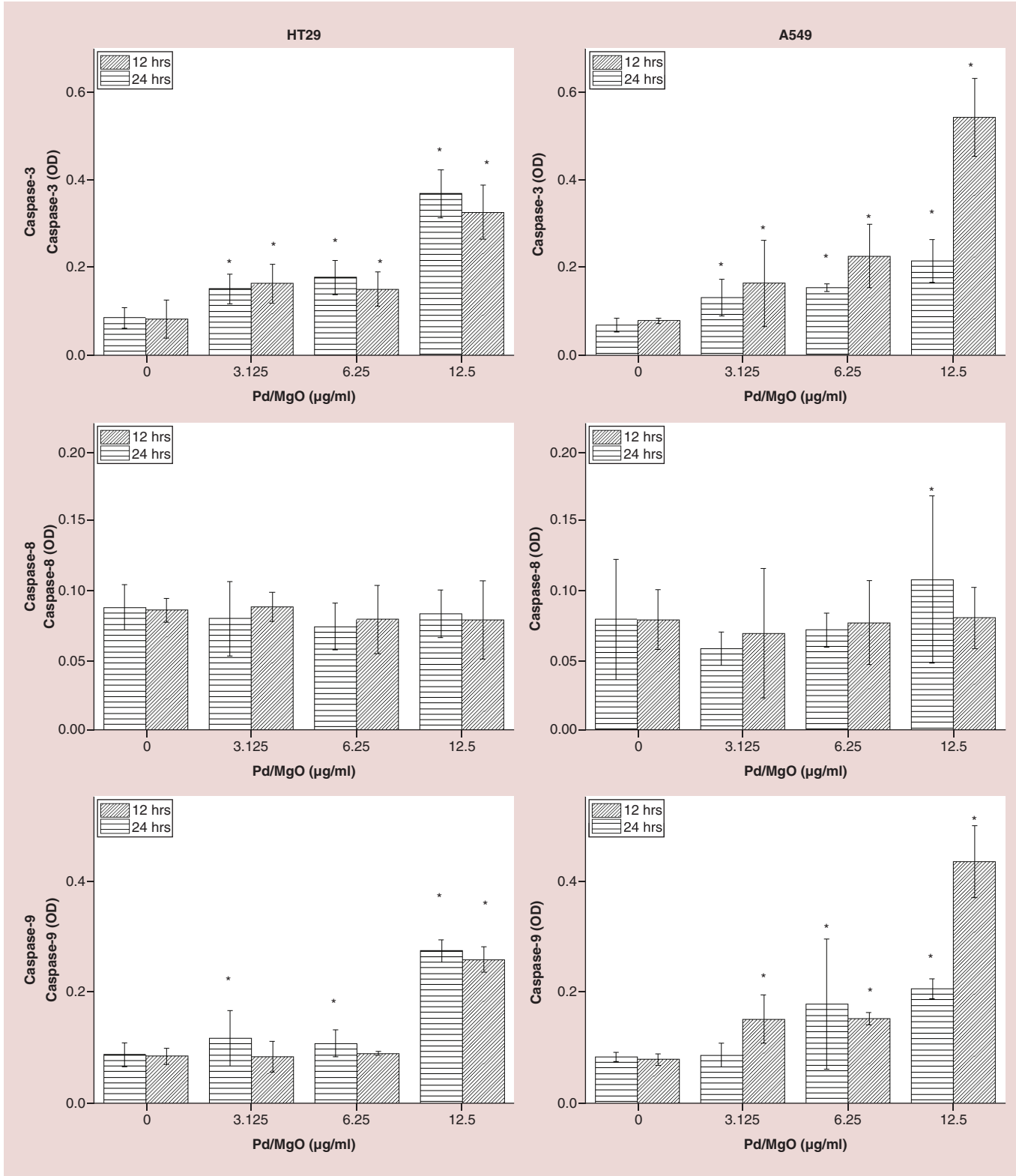

Figure 4. Effect of Palladium-doped magnesia nanoparticles on human colorectal adenocarcinoma and lung adenocarcinoma cell line caspase-3, -8 and -9 activities after 12- and 24-h exposure. Values are mean ± standard deviation (n = 3 well/treatment).
*$p < 0.05$ compared with nontreated cells.
A549: Human breast adenocarcinoma; HT29: Human colorectal adenocarcinoma cell line; OD: Optical density; Pd/MgO: Palladium-doped magnesia.

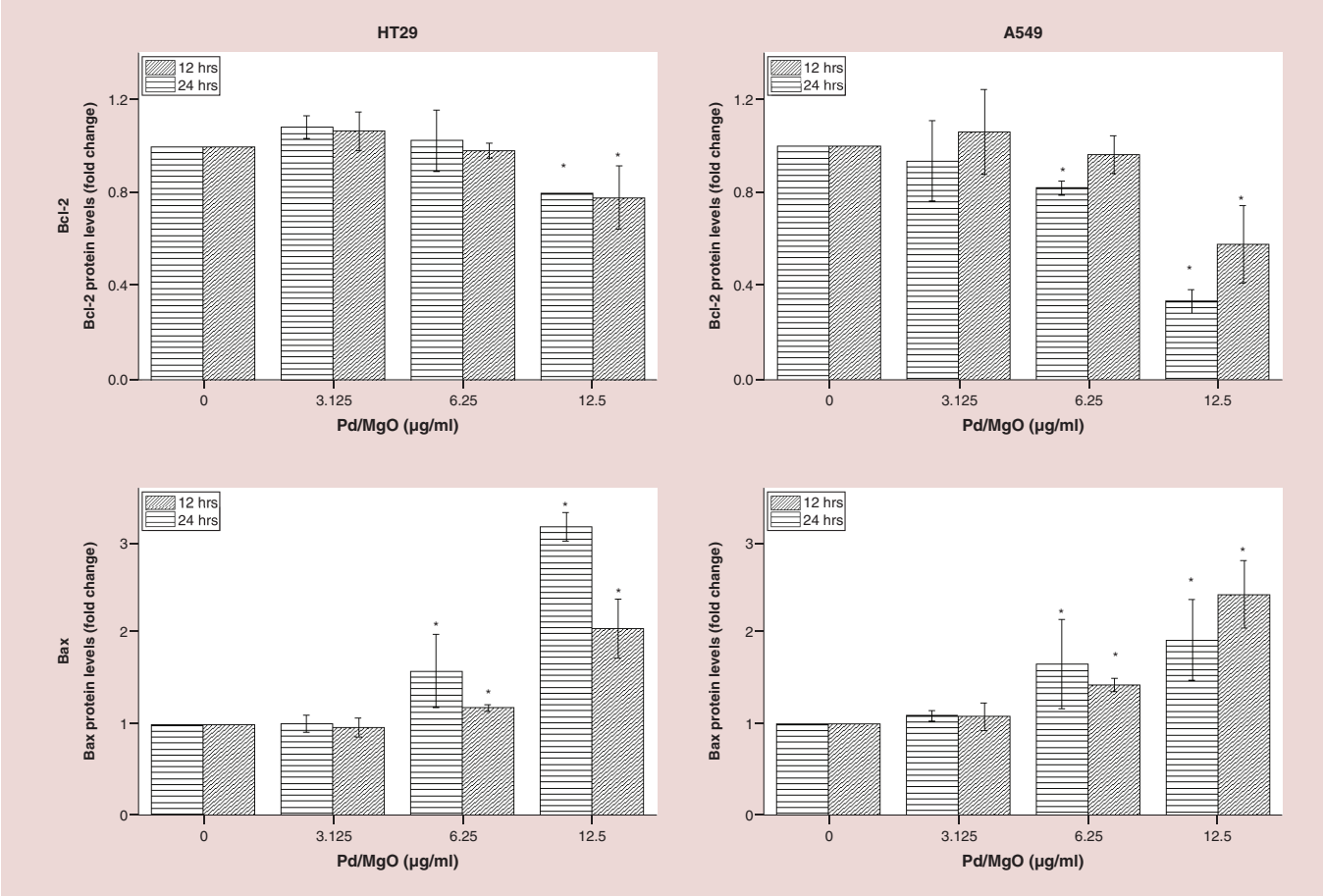

Figure 5. Effect of Palladium-doped magnesia nanoparticles on Bcl-2, Bax and p53 proteins expressions and cytochrome C release in human colorectal adenocarcinoma and lung adenocarcinoma cell line after 12- and 24-h exposure. Values are mean ± standard deviation (n = 3 well/treatment).
*$p < 0.05$ compared with nontreated cells.
A549: Human breast adenocarcinoma; HT29: Human colorectal adenocarcinoma cell line; Pd/MgO: Palladium-doped magnesia.

Cytochrome C

The effects of Pd/MgO nanoparticles on cytochrome C release by HT29 and A549 cells were generally similar (Figure 5). The nanoparticles increase cytochrome C release by HT29 and A549 early at 12 h. However, in the case of A549 cells after 24-h exposure, only the high concentration (12.5 µg/ml) of Pd/MgO nanoparticles showed significantly high ($p < 0.05$) cytochrome C release. The lower nanoparticle concentration did not have significant effect ($p > 0.05$) on A549 cells.

Morphological examination

The A549 lung cancer and HT29 colon cancer cells treated with 24-h Pd/MgO nanoparticles IC_{50} concentration showed shrinkage and membrane blebbing (Figure 6). By the morphological changes, the Pd/MgO nanoparticles seemed to be more potent at inducing apoptosis of the A549 than HT29 cells. Nontreated cells, even after 24 h, were in nearly complete monolayered and uniformly distributed in the culture plates. Morphologically, the nontreated cells were either round or oblong, suggesting that they are intact.

Discussion

The study focused on the synthesis and characterization of Pd/MgO nanoparticles and determination of the cytotoxic effects on cancer cells using sustainable, low-toxic materials, and energy-saving synthetic methodologies. XRD is the primary method for determination of diameter of nanocrystalline powdered materials [19]. In this study, XRD was used to determine the crystalline phase and orientation of atoms in Pd/MgO nanoparticles. The

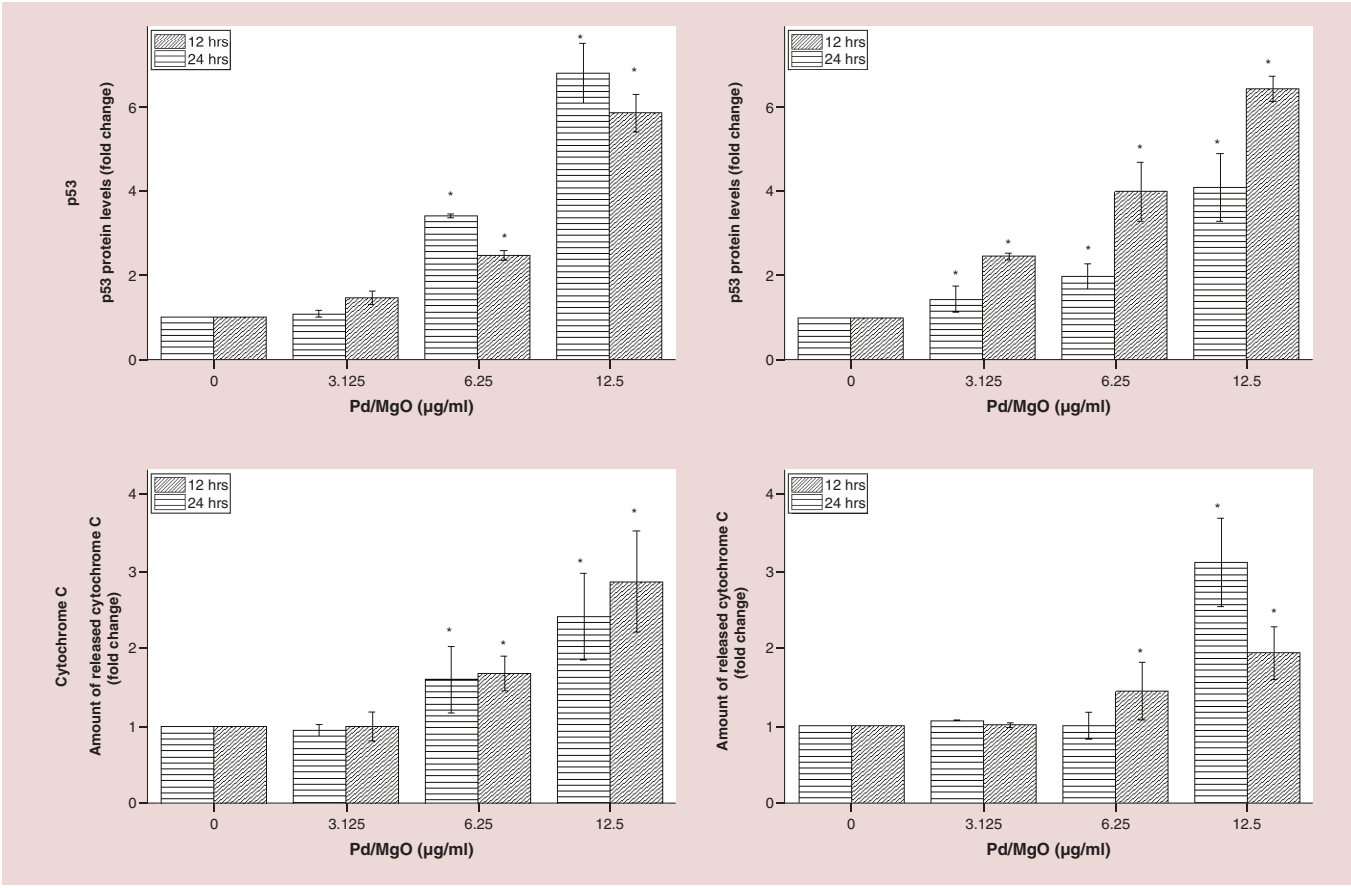

Figure 5. Effect of Palladium-doped magnesia nanoparticles on Bcl-2, Bax and p53 proteins expressions and cytochrome C release in human colorectal adenocarcinoma and lung adenocarcinoma cell line after 12- and 24-h exposure (cont.). Values are mean ± standard deviation (n = 3 well/treatment).
*$p < 0.05$ compared with nontreated cells.
A549: Human breast adenocarcinoma; HT29: Human colorectal adenocarcinoma cell line; Pd/MgO: Palladium-doped magnesia.

Figure 6. Effect of treatment with IC_{50} concentration of Palladium-doped magnesia nanoparticles on the human colorectal adenocarcinoma and lung adenocarcinoma cell lines after 24 h. Apoptotic cells showed the characteristic morphological features, including loss of membrane asymmetry and cell shrinkage and typical membrane blebbing (Black arrow) (200×).
A549: Human breast adenocarcinoma; HT29: Human colorectal adenocarcinoma cell line.

characterization did not show any peak that is associated with impurities; thus, the final Pd/MgO nanoparticles were pure. FTIR data determines absorption, and transmittance at IR wavelengths as a means of determining chemical composition of Pd/MgO nanoparticles [20] and based on the analysis, the chemical bond in the Pd/MgO nanoparticles was clearly evident, suggesting that they are stable.

Based on SEM and TEM ultrastructure, the size distribution of Pd/MgO nanoparticles is between 44 and 85 nm. The ball mill is used to reduce the size of metallic particles [21,22]. Changing the annealing and calcination temperatures reduces the size of Pd/MgO nanoparticles [23]. The palladium-doped magnesia nanoparticles tend to aggregate into dense masses and this can compromise their performance as an anticancer agent. Current available techniques to disaggregate the nanoparticles do not always produce consistent results and may not be useful. In fact, sonication at an energy level high enough to disaggregate the particles or the inclusion of albumin or serum as a stabilizer may be better alternatives for the production of usable nanoparticles [24].

The Pd/MgO nanoparticles are small enough to evade the mononuclear phagocytic system, allowing for a prolonged circulatory period, a characteristic ideal for therapeutic compound complexes. Palladium is shown to have some anticancer properties. It was shown that palladium–diethyldithiocarbamate complex caused cancer cell death. Pd (II) induced G2/M phase arrest in the hepatocellular carcinoma, HepG2 and S phase arrest in the esophageal squamous carcinoma, Kyse-30, cell lines [25]. Palladium in complex with ethylenediamine and pyridine content show effects similarly to that produced by cisplatin on the human leukemia cell line [26]. Pd/MgO nanoparticles with properties similar to the above complexes, are antiproliferative toward the colon, HT29, and lung, A549, cancer cells.

It seemed that Pd/MgO nanoparticles are not selective toward the lung cancer cells, because it is also toxic to normal lung cells. It is suggested the Pd/MgO nanoparticles affect cancer and normal cells in a similar way, which is through the inhibition of cell replication. Thus, the Pd/MgO nanoparticles would be very antiproliferative toward fast-dividing cells such cancer cells, hepatocytes, and leukocytes and less so toward the slow-dividing normal cells.

Apoptosis occurs via either the intrinsic or extrinsic pathways, or both. Caspases play vital roles in the apoptotic pathways [27]. Caspase-9 is the main mediator for the intrinsic while caspase-8 is for the extrinsic pathway. Both pathways activate the executioner caspase-3, -6 and -7 to induce apoptosis [28]. Pd/MgO nanoparticles had the greatest effect on the stimulation of caspases-3 and -9 activities and not as significant on the caspase-8 activity of the HT29 and A549 cells. This suggests the apoptotic effect of Pd/MgO nanoparticles is mainly through the intrinsic pathway and mediated through the mitochondrial activity. This was evident by downregulation of Bcl-2 and upregulation of the Bax protein and increase in release of cytochrome C in these cancer cells [29], as the result of Pd/MgO nanoparticle treatments. The anticancer effect of Pd/MgO nanoparticles is accentuated by the increase in expression of p53 tumor suppressor protein in the cancer cells.

Evidently, this study showed that the Pd/MgO nanoparticle is a potential efficacious anticancer agent. The antiproliferative effect of Pd/MgO nanoparticles is suggested to occur primarily through the induction of intrinsic apoptosis pathway.

Conclusion

The Pd/MgO nanoparticles were between 47 and 70 nm in size. The *in vitro* cytotoxicity assay showed that the human HT29 colon and lung A549 cancer, and normal MRC-5 lung cells were all variably susceptible to the cytotoxic effect of Pd/MgO nanoparticles. It appears that the anticancer effects of Pd/MgO nanoparticles implicated the caspase-9, Bcl-2 family of proteins and cytochrome C release, suggesting that the mode of death induced by Pd/MgO nanoparticles is via the intrinsic/mitochondrial pathway. The anticancer effect of Pd/MgO nanoparticles was accentuated by the activation of the tumor suppressor protein, p53. In conclusion, Pd/MgO nanoparticles is an effective antiproliferative agent for human colon and lung cancer cell lines.

Financial & competing interests disclosure

The authors have no relevant affiliations or financial involvement with any organization or entity with a financial interest in or financial conflict with the subject matter or materials discussed in the manuscript. This includes employment, consultancies, honoraria, stock ownership or options, expert testimony, grants or patents received or pending, or royalties.

No writing assistance was utilized in the production of this manuscript.

References

Papers of special note have been highlighted as: • of interest; •• of considerable interest

1. Pecorino L. *Molecular Biology of Cancer: Mechanisms, Targets, and Therapeutics.* OUP Oxford, UK (2012).
2. Macdonald F, Ford C, Casson A. *Molecular Biology of Cancer.* Taylor & Francis, London, UK (2004).
3. Al-Qubaisi M, Rozita R, Yeap S-K, Omar A-R, Ali A-M, Alitheen NB. Selective cytotoxicity of goniothalamin against hepatoblastoma HepG2 cells. *Molecules* 16(4), 2944–2959 (2011).

Summary points

- Co-precipitation method from aqueous solution is a promising approach in the synthesis of palladium-doped magnesia (Pd/MgO) nanoparticles.
- Scanning electron microscopy images showed that the Pd/MgO nanoparticle had uniform size distribution and cuboid in structure.
- X-ray diffraction and Thermogravimetric analysis (TGA) showed that the nanoparticles were pure and thermally stable.
- Treatment with our nanoparticles resulted in death of cancer cells.
- Pd/MgO nanoparticles are selective toward the colon cancer cells when compared with normal colon cells.
- Nanoparticles induced apoptosis primarily via caspase-9-dependent mitochondrial signaling pathway.
- Downregulation of Bcl-2, upregulation of Bax and p53 proteins and increase in release of cytochrome C in cancer cells occurred as the result of Pd/MgO nanoparticle treatments.
- Cancer cells treated with Pd/MgO nanoparticles showed shrinkage, membrane blebbing and loss of cell membrane integrity.

4. Al-Qubaisi M, Rasedee A, Flaifel M *et al.* Characterization of thymoquinone/hydroxypropyl-β-cyclodextrin inclusion complex: application to anti-allergy properties. *Eur. J. Pharm. Sci.* 133, 167–182 (2019).

•• **Shows serious issue of poor aqueous solubility of drugs in medical application and development of anticancer compounds.**

5. Dabrowiak JC. *Metals in Medicine.* Wiley, West Sussex, UK (2013).

6. Prestayko AW. *Cisplatin: Current Status and New Developments.* Elsevier Science, NY, USA 445–458 (2013).

7. Markowska A, Kasprzak B, Jaszczyńska-Nowinka K, Lubin J, Markowska J. Noble metals in oncology. *Contemp. Oncol.* 19(4), 271 (2015).

• **Determines the role and mechanism of noble metals in cancer treatment and their limitations.**

8. Jamieson ER, Lippard SJ. Structure, recognition, and processing of cisplatin– DNA adducts. *Chem. Rev.* 99(9), 2467–2498 (1999).

9. Rosell R, Danenberg KD, Alberola V *et al.* Ribonucleotide reductase messenger RNA expression and survival in gemcitabine/cisplatin-treated advanced non-small cell lung cancer patients. *Clin. Cancer Res.* 10(4), 1318–1325 (2004).

10. Cullen KJ, Yang Z, Schumaker L, Guo Z. Mitochondria as a critical target of the chemotheraputic agent cisplatin in head and neck cancer. *J. Bioenerg. Biomembr.* 39(1), 43–50 (2007).

11. Campbell KC, Rybak LP, Meech RP, Hughes L. D-methionine provides excellent protection from cisplatin ototoxicity in the rat. *Hear. Res.* 102(1-2), 90–98 (1996).

12. Kröning R, Lichtenstein A, Nagami G. Sulfur-containing amino acids decrease cisplatin cytotoxicity and uptake in renal tubule epithelial cell lines. *Cancer Chemother. Pharmacol.* 45(1), 43–49 (2000).

• **Reveals the serious side effects of chemotherapies on human health, which in turn, encourage ongoing search for more selective anticancer drugs with minimal side effects.**

13. Zhen X, Wang X, Xie C, Wu W, Jiang X. Cellular uptake, antitumor response and tumor penetration of cisplatin-loaded milk protein nanoparticles. *Biomaterials* 34(4), 1372–1382 (2013).

•• **Nanotechnology and nanomedicine are promising strategies employed in the development of anticancer drugs.**

14. Kundu M, Sadhukhan P, Ghosh N *et al.* pH-responsive and targeted delivery of curcumin via phenylboronic acid-functionalized ZnO nanoparticles for breast cancer therapy. *J. Adv. Res.* 18, 161–172 (2019).

•• **Using transition metal oxide as drug carrier offers an improved, targeted tumor therapy strategy for cancer treatment without less side effect.**

15. Soudée E, Péra J. Mechanism of setting reaction in magnesia-phosphate cements. *Cement Concrete Res.* 30(2), 315–321 (2000).

16. Al-Doghachi FJA. Effects of platinum and palladium metals on Ni/Mg1-xZrxO catalysts in the CO2 reforming of methane. *Bull. Chem. React. Eng. Catalysis* 13(2), 295–310 (2018).

•• **The loading of transition metal oxide with Palladium exhibit more active site on the nanoparticles surface.**

17. Al-Qubaisi MS, Rasedee A, Flaifel MH *et al.* Induction of apoptosis in cancer cells by NiZn ferrite nanoparticles through mitochondrial cytochrome C release. *Int. J. Nanomed.* 8, 4115–4130 (2013).

18. Al-Qubaisi MS, Rasedee A, Flaifel MH *et al.* Cytotoxicity of nickel zinc ferrite nanoparticles on cancer cells of epithelial origin. *Int. J. Nanomed.* 8, 2497–2508 (2013).

19. Suryanarayana C, Norton MG. *X-Ray Diffraction: A Practical Approach.* Springer Science and Business Media, NY, USA (2013).

20. Moore E. *Fourier Transform Infrared Spectroscopy (FTIR): Methods, Analysis and Research Insights.* Nova Science Publishers, Incorporated, NY, USA (2016).

21. Tsuzuki T, Mccormick PG. Mechanochemical synthesis of metal sulphide nanoparticles. *Nanostruct. Mater.* 12(1-4), 75–78 (1999).

22. US20060153728 (2006)

23. Mohammadi FM, Ghasemi N. Influence of temperature and concentration on biosynthesis and characterization of zinc oxide nanoparticles using cherry extract. *J. Nanostruct. Chem.* 8(1), 93–102 (2018).

24. Bihari P, Vippola M, Schultes S *et al.* Optimized dispersion of nanoparticles for biological in vitro and in vivo studies. *Particle Fibre Toxicol.* 5(1), 14 (2008).

• **Recommendation to reduce nanoparticle aggregation, which leads to increase drug efficacy.**

25. Hadizadeh S, Najafzadeh N, Mazani M, Amani M, Mansouri-Torshizi H, Niapour A. Cytotoxic effects of newly synthesized palladium (II) complexes of diethyldithiocarbamate on gastrointestinal cancer cell lines. *Biochem. Res. Int.* 2014, 813457–813457 (2014).

26. Pranczk J, Jacewicz D, Wyrzykowski D, Chmurzynski L. Platinum (II) and palladium (II) complex compounds as anti-cancer drugs. Methods of cytotoxicity determination. *Curr. Pharm. Analysis* 10(1), 2–9 (2014).

•• **Good introduction for using palladium in cancer treatment and its side effects.**

27. Cohen GM. Caspases: the executioners of apoptosis. *Biochem. J.* 326(1), 1–16 (1997).

28. Nicholson DW, Thornberry NA. Caspases: killer proteases. *Trends Biochem. Sci.* 22(8), 299–306 (1997).

29. Reed JC, Green DR. *Apoptosis: Physiology and Pathology.* Cambridge University Press, NY, USA (2011).